

La2010: A new orbital solution for the long term motion of the Earth.

J. Laskar¹, A. Fienga^{1,2}, M. Gastineau¹, and H. Manche¹

¹ ASD, IMCCE-CNRS UMR8028, Observatoire de Paris, UPMC, 77 Av. Denfert-Rochereau, 75014 Paris, France

² Observatoire de Besançon-CNRS UMR6213, 41bis Av. de l'Observatoire, 25000 Besançon

May 29, 2018

Abstract. We present here a new solution for the astronomical computation of the orbital motion of the Earth spanning from 0 to -250 Myr. The main improvement with respect to the previous numerical solution La2004 (Laskar et al. 2004) is an improved adjustment of the parameters and initial conditions through a fit over 1 Myr to a special version of the high accurate numerical ephemeris INPOP08 (Fienga et al. 2009). The precession equations have also been entirely revised and are no longer averaged over the orbital motion of the Earth and Moon. This new orbital solution is now valid over more than 50 Myr in the past or in the future with proper phases of the eccentricity variations. Due to chaotic behavior, the precision of the solution decreases rapidly beyond this time span, and we discuss the behavior of various solutions beyond 50 Myr. For paleoclimate calibrations, we provide several different solutions that are all compatible with the most precise planetary ephemeris. We have thus reached the time where geological data are now required to discriminate among planetary orbital solutions beyond 50 Myr.

1. Introduction

Due to gravitational planetary perturbations, the elliptical elements of the orbit of the Earth are slowly changing in time, as is the orientation of the planet's spin axis. As described by (Milankovitch 1941) these changes induce variations of the insolation received on the Earth's surface that are at the origin of large climatic changes. Since the work of (Hays et al. 1976), that established a correlation between astronomical forcing and the $\delta^{18}O$ records over the past 500 kyr, there has been a increasing need for precise long term ephemeris for the Earth orbital and rotational evolution (see Laskar et al. (2004) for a more detailed historical account).

For paleoclimate studies, the most widely used orbital solutions are nowadays either the averaged solution of (Laskar 1988; Laskar et al. 1993b) or the most recent numerical solution of Laskar et al. (2004).

The first long term direct numerical integration (without averaging) of a realistic model of the Solar system, together with the precession and obliquity equations, was made by (Quinn et al. 1991) over 3 Myr. Over its range, this solution presented small differences with the secular solution of (Laskar 1988, 1990), (see Laskar et al. (1992)). The orbital motion of the full Solar system has then been computed over 100 Myr by (Sussman & Wisdom 1992), using a symplectic integrator with mixed variables (Wisdom

& Holman 1991), confirming the chaotic behavior found by Laskar (1989, 1990). Following the improvement of computer technology, long term integrations of realistic models of the Solar system have improved (Varadi et al. 2003; Laskar et al. 2004), but the main limitation remains the exponential divergence of nearby orbits resulting from the chaotic motion of the Solar system (Laskar 1989, 1990, 1999). Although it is now possible to integrate the motion of the Solar system over time periods of more than 5 Gyr, comparable to its age or expected life time (Laskar & Gastineau 2009), it is clear that the chaotic behavior of the solution will still limit its validity to a few tens of Myr.

The present paper is a continuation of the work that has been conducted for decades in our group in order to obtain the most precise solution for the past evolution of the orbit and rotational state of the Earth, aimed to paleoclimate studies.

The numerical integrator is the same symplectic integrator from (Laskar & Robutel 2001) as the one used in the La2004 solution (Laskar et al. 2004), but it was entirely rewritten in C in order to access to extended precision on the intel architecture. On the other hand, the tidal model has been largely modified, and is now close to the one used in the JPL planetary ephemeris DE405 (Standish 1998b) or in our new planetary ephemeris INPOP (Fienga et al. 2008, 2009). The precession equations for the evolution of the spin axis of the Earth are also new (Boué & Laskar

Send offprint requests to: J. Laskar, e-mail: laskar@imcce.fr

2006). There are no longer averaged over the orbital motion of the planets, and allow a precise computation of the evolution of the Earth spin axis that can be compared to the most precise model adopted by the IAU (Soffel *et al.* 2003) (see Fienga *et al.* 2008).

In previous long term solutions Laskar (1988); Quinn *et al.* (1991); Laskar *et al.* (1993a); Varadi *et al.* (2003); Laskar *et al.* (2004), the initial conditions of the solutions were obtained either directly from a high precision planet ephemeris, or by a fit over its full time span (as in La2004) that was still limited to a few thousands of years. It was thus difficult to monitor the real uncertainty of the used ephemeris.

In the present work, we have profoundly removed this limitation. Indeed, in the past few years, we have entirely build a new high precision planetary ephemeris INPOP that has been fitted to all available planetary and Lunar observations (Fienga *et al.* 2008, 2009). This ephemeris that has been released already in two versions (INPOP06 and INPOP08) is thus equivalent to the JPL ephemerides DE that were used for determining the initial conditions of the previous long term solutions. In addition, we have removed in INPOP all time limitations and carefully designed the numerical integrator. We could thus extend the integration of INPOP06 and INPOP08 over 1 Myr with the full ephemeris model. The initial conditions of the present long term ephemeris could then be fitted over an extended interval of several hundreds of thousands of years before being extended to 250 Myr. By doing so, we were able to take into account the full precision of the ephemeris, and it appears now that the limitations is no longer in the model but in the planetary observations themselves.

The first sections of this paper (sec 2 to sec 6) describe successively the La2010 numerical model, its link with the INPOP ephemeris, the various La2010 solutions and their comparison with the high precision INPOP ephemeris and the previous La2004 solution. The following sections (7 to 9) are focussed on the long term cycles that are present in the eccentricity solution and their stability. This topic is of essential importance for the attempt to establish an astronomically calibrated geological timescale (see Pälike & Hilgen 2008) . Indeed, the La2004 solution (Laskar *et al.* 2004) has been successfully used for the astronomical calibration of the Neogene period (≈ 23 Myr) (Lourens *et al.* 2004) that is included in the most recent standard timescale GTS2004 (Gradstein *et al.* 2004). At present, there is a continuous effort to improve this timescale and to extend the astronomical calibration to the full Cenozoic period (≈ 65 Myr) through the Earthtime and Earthtime-eu projects (<http://www.earthtime.org>, <http://earthtime-eu.eu>). In order to do so, the length of validity of the orbital solution has to be extended by more than 20 Myr. Because of the chaotic behavior of the solution (Laskar 1989), this corresponds to improve the precision of the model and parameters by two orders of magnitude, and the present work is an attempt in this direction.

On the other hand, beyond the horizon of predictability of the orbital solution, it is tempting to use the recorded geological information to provide constraints on the orbital motion of the Solar System (Lourens *et al.* 2001; Pälike *et al.* 2004). Due to the lack of precision of the geological data in remote periods of time, this can only be done through macroscopic aspects of the orbital solution. The analysis of the secular resonance $g_4 - g_3 - 2(s_4 - s_3)$ (Sec. 8) is devoted to this problem. In particular, it is shown how the analysis of the modulation of the amplitude of the 405 kyr eccentricity term can discriminate among various orbital solutions and thus provide feedback from geological data to astronomical models.

2. Numerical model

The orbital solutions La90-93 (Laskar 1990; Laskar *et al.* 1993a) were obtained by a numerical integration of the averaged equations of the Solar system, including the main general relativity and Lunar perturbations. As computer technology now allows to integrate directly precise models of the evolution of the Solar System over several hundreds of Myr, we have decided, since La2004 (Laskar *et al.* 2004) to use direct integrations, without averaging.

The dynamical model and numerical integrators are very close to the ones of La2004. We will thus refer to (Laskar *et al.* 2004) for a detailed description of these models, and will only report here the elements that are different in the present model and integration.

2.1. Dynamical model

The orbital model comprises all 8 planets of the Solar system, and Pluto. The post-Newtonian general relativity corrections of order $1/c^2$ due to the Sun are included following Saha & Tremaine (1994). The Moon is treated as a separate object. In order to obtain a realistic evolution of the Earth-Moon system, we also take into account the most important coefficient in the gravitational potential of the Earth and of the Moon, and the tidal dissipation in the Earth-Moon System (Laskar *et al.* 2004). Contrary to La2004, the precession and obliquity are now integrated without averaging over the orbital periods following (Boué & Laskar 2006). In the final runs, we have also added the contribution of the main 5 minor planets and some small correction to precession motions are made to take into account the remaining asteroids or other unmodeled parameters.

2.2. Numerical integrator

As in La2004, the numerical integration was performed with the symplectic integrator scheme $SABAC_4$ (Laskar & Robutel 2001), with a correction step for the integration of the Moon. This integrator is particularly adapted to perturbed systems where the Hamiltonian governing the equations of motion can be written as the sum

of an integrable part (the Keplerian equations of the planets orbiting the Sun and of the Moon around the Earth), and a small perturbing potential representing the interactions among the planets.

The step size used in the integration is $\tau = 5 \times 10^{-3} \text{yr} = 1.82625 \text{ days}$, while for La2010a, $\tau = 10^{-3} \text{yr} = 0.36525 \text{ days}$. The initial conditions of the integration were least square adjusted to a special version of INPOP that has been extended in time over 1 Myr. Depending on the solution, this fit was performed over 1 Myr or 580 kyr (see Tab. 2).

In La2004, the integration was made in double precision, with machine Epsilon $\varepsilon_M \approx 2.22 \times 10^{-16}$. Here, we have integrated the solutions in extended precision on Xeon Intel processors, which allows arithmetics in 80 bits instead of 64 bits in double precision. The machine Epsilon becomes then $\varepsilon'_M \approx 1.1 \times 10^{-19}$.

The integration time for our complete model, including 5 asteroids and the Moon as a separate object with $\tau = 5 \times 10^{-3} \text{yr}$ is about one day per 3 Myr in extended precision, and one day per 6 Myr in double precision on a Intel Xeon E5462 2.8 Ghz workstation. When the step size is decreased to $\tau = 10^{-3} \text{yr}$, for the nominal solution La2010a, the requested time is 5 days for 3 Myr, and more than one year for the whole integration.

2.3. Numerical error

As in La2004, the numerical error is estimated by comparing two integrations with the same model and slightly different step size. For the nominal solution, we use $\tau = 5 \times 10^{-3} \text{ yr}$, and for the alternate solution $\tau^* = 4.8828125 \times 10^{-3} \text{ years}$. This special value is chosen in order that our output time span $h = 1000 \text{ years}$ corresponds to an integer number (204800) of steps, in order to avoid any interpolation problems in the check of the numerical accuracy. With $\tau = 10^{-3} \text{yr}$, we have then $\tau^* = 0.9765625 \times 10^{-3} \text{yr}$ (Tab. 2).

2.3.1. Rotational evolution

Contrarily to La2004, the precession equations are no longer averaged over the orbital motion of the planets or the Moon, but are treated in a vectorial manner, following (Boué & Laskar 2006). Following (Darwin 1880; Mignard 1979), we assume that the torque resulting from tidal friction is proportional to the time lag Δt needed for the deformation to reach the equilibrium. This time lag is supposed to be constant, and the angle between the direction of the tide-raising body and the direction of the high tide (which is carried out of the former by the rotation of the Earth) is proportional to the speed of rotation. Such a model is called “viscous”, and corresponds to the case for which $1/Q$ is proportional to the tidal frequency.

Various additional small dissipative effects as core–mantle friction (Poincaré 1910; Rochester 1976; Lumb & Aldridge 1991; Correia *et al.* 2003), atmospheric tides

(Chapman & Lindzen 1970; Volland 1978; Correia & Laskar 2003), mantle convection (Forte & Mitrovica 1997), climate friction (Rubincam 1990, 1995; Bills 1994; Ito *et al.* 1995; Levrard & Laskar 2003), have been discussed in La2004, but their effects are considered to be too small and too uncertain to be added in the model, as it was the case for La2004.

3. The numerical ephemeris INPOP

The initial conditions of La2004 were obtained by adjustment to the JPL numerical ephemeris DE406 (Standish 1998a) over the full range of DE406, that is from -5000 yr to $+1000 \text{ yr}$ from the present date. DE406 is itself adjusted to planetary observations.

With this procedure, we are limited by the range of the available ephemeris, and in general, the latest ephemeris is not always computed over a long time interval. For example, the most recent ephemeris from JPL, DE421 (Folkner 2008), has only been provided over the time interval $[1900, 2050] \text{ yr}$. Moreover, it is difficult to estimate the true uncertainty of the provided ephemeris. Most often, this uncertainty is only revealed with the publication of the new ephemeris that can be compared with the previous one. In order to overcome these limitations, we have undertaken in our group the construction of a full size planetary and lunar ephemeris. After five years of work, the solutions are now mature and two successive versions have already been published : INPOP06 (Fienga *et al.* 2008) and INPOP08 (Fienga *et al.* 2009). The detailed information about the dynamical models and fit to available observations can be found in the related publications.

We have removed in the construction of these ephemerides all elements that would limit the length of validity of the solutions. In particular, we have not used some precession formulas for the evolution of the spin axis of the Earth. Instead, we have integrated together with the full ephemeris, a precession model for the Earth that is obtained after averaging over the rotation period of the Earth, but not over the orbital period of the Earth or of the Moon (Fienga *et al.* 2008).

The full ephemeris could then be prolonged over 1 Myr using extended precision 80 bits arithmetics with the Adams integrator of INPOP. This integration took about 4 month of CPU on an itanium 9040 1.6 Ghz workstation. This process was first made for INPOP06, and then for INPOP08, when the final version of this latest ephemeris (Fienga *et al.* 2009) was finally made available. These highly accurate ephemerides are then used for the calibration and evaluation of the long models La2010.

We refer to (Fienga *et al.* 2008, 2009) for a precise description of INPOP06 and INPOP08. With respect to INPOP06, INPOP08 benefitted from several additional sets of observations. The Mars Express and Venus Express ranging data provided very precise measures of Earth–Mars and Earth–Venus distances with a precision of a few meters (Fienga *et al.* 2009). For Mars, this was a continuation of a long sequence of very precise measures that

Table 1. Maximum difference between INPOP06 and INPOP08 over 1 Myr (top). and between INPOP08 (computed in extended precision) and INPOP08d, a version of INPOP08 computed in double precision, over 1 Myr (bottom).

| | INPOP06-INPOP08 | | |
|---------|------------------|-----------------|-----------------|
| | $a \times 10^6$ | $e \times 10^6$ | $i \times 10^6$ |
| Mercury | 0.027 | 25.544 | 12.598 |
| Venus | 0.543 | 4.746 | 6.299 |
| EMB | 1.067 | 4.709 | 4.029 |
| Mars | 3.852 | 7.134 | 2.570 |
| Jupiter | 56.126 | 20.542 | 0.577 |
| Saturn | 585.092 | 76.138 | 1.315 |
| Uranus | 885.497 | 92.313 | 1.481 |
| Neptune | 3449.727 | 104.593 | 0.882 |
| Pluto | 19900.821 | 297.483 | 46.579 |
| Moon | 57.345 | 42006.038 | 1463.465 |
| | INPOP08-INPOP08d | | |
| | $a \times 10^6$ | $e \times 10^6$ | $i \times 10^6$ |
| Mercury | 0.012 | 0.077 | 0.011 |
| Venus | 0.640 | 1.706 | 0.138 |
| EMB | 0.889 | 1.768 | 0.125 |
| Mars | 6.899 | 6.081 | 0.394 |
| Jupiter | 1.004 | 0.175 | 0.009 |
| Saturn | 2.542 | 0.243 | 0.007 |
| Uranus | 6.834 | 0.333 | 0.006 |
| Neptune | 13.479 | 0.415 | 0.008 |
| Pluto | 25.332 | 0.455 | 0.061 |
| Moon | 29.594 | 12400.799 | 527.701 |

Note. EMB is the Earth-Moon barycenter. The semi-major axis a is in AU and the inclination with respect to the invariable plane i is in radians.

had been acquired with the Martian spacecrafts since the first Viking landers on Mars, but for Venus, the new ranging data processed by ESOC were the first highly accurate estimates of the Earth-Venus distance which uncertainty was thus reduced from a few hundred meters to a few meters (Fienga et al. 2009). Another improvement in INPOP08 consists in the use of some Cassini normal points (Folkner 2008) that also help to constrain the position of Saturn. In addition, in INPOP08, the Lunar orbit was fitted to Lunar laser ranging data in a consistent way, while in INPOP06, the fit of the Lunar ephemeris was only made with respect to Lunar distances given by DE405 (Standish 1998a).

It is always difficult to estimate the true uncertainty of an ephemeris. In (Fienga et al. 2009), this estimate is obtained by comparison with INPOP06 and DE421 over 10 and 100 years. The differences between INPOP08 and DE421 are in general smaller, but comparable with the differences INPOP08-INPOP06, with the notable exception of the positions of Saturn, where the differences INPOP08-DE421 are one order of magnitude smaller than the differences INPOP08-INPOP06. This is certainly the consequence of the use in both DE421 and INPOP08 of the new Cassini data that constrain very much the position of Saturn.

After 100 yr, the differences INPOP08-DE421 in barycentric positions range from a few kilometers for the inner planets to a few thousands km for the outer planets, and only 40 km for Saturn (Fienga et al. 2009, Tab. 6). This is several order of magnitude more than the error coming from the numerical integration (Fienga et al. 2008, Tab. 1) that reach only a few micrometers after the same range, and less than a few meters after 10000 yr. It can thus be assumed that after one million year, the numerical error in the integration of INPOP will still be smaller than the propagation of the uncertainty of the model and parameters, obtained by the fit to planetary positions.

We have thus prolonged the two INPOP ephemeris (INPOP06 and INPOP08) over 1 Myr in order to use these solutions as a starting point for the long term ephemeris. The accuracy of these solutions after 1 Myr is then evaluated by the comparison of INPOP06 to INPOP08, with the assumption that the real uncertainty of INPOP08 will be smaller than the difference INPOP08-INPOP06 (Table 1). In Table 1, we also provide the differences of two integrations of INPOP08 made in double precision and in extended precision, in order to evaluate the numerical precision of the integration. From the comparisons made in (Fienga et al. 2008), we can assume that the error on the integration of INPOP08 made in extended precision is in fact several orders of magnitude smaller than the differences reported in this table.

4. Successive versions of La2010

The process leading to a long term solution is long, as we had to wait first for the INPOP solution to be ready over 1 Myr, and then only we could make the fit of the long term model. After that, the integration of the long term model over 250 Myr in extended precision still required about 3 months of CPU time, and more than one year when the step size is reduced to 10^{-3} yr. This is why we have performed several versions of these long term ephemeris, that could be used for comparisons, and also to study the stability of the solution with respect to improvement of the INPOP ephemeris. As the INPOP08 ephemeris was only finished very recently, some of the solutions fitted to INPOP08 have been fitted over only 580 kyr instead of 1 Myr for INPOP06, but this did not make a large difference, and the solutions are still at the end compared to INPOP08 over 1Myr as the integration of INPOP08 has now reached 1Myr. The various models that have been selected are summarized in Table 2.

The solution La2010d has been fitted to INPOP06 over 1 Myr, while the more recent solutions La2010a, La2010b, La2010c, and their associated solutions La2010a*, La2010b*, La2010c*, have been fitted over INPOP08, over 580 kyr for the solutions with index a,b, and over 1 Myr for La2010c and La2010c*. All these models, except La2010c and La2010c* comprise the five major asteroids, Ceres, Vesta, Pallas, Iris and Bamberga.

In all cases, the parameters are taken from the corresponding INPOP ephemeris, as well as the starting value

Table 2. Variants of the La2010 solutions. The nominal solution La2010a is obtained for a stepsize $\tau = 1 \times 10^{-3}$ in extended precision. The other solutions, with different setting have been computed to test the stability of the nominal solution.

| name | files | ephem | fit | τ (yr) | prec | |
|----------|--------------|----------|----------|----------------------------|------|--------|
| La2010a | ast5AL08cxc | INPOP08a | 0.58 Myr | 1×10^{-3} | Ext | 5ast,M |
| La2010a* | ast5AL08czc | INPOP08a | 0.58 Myr | 0.9765625×10^{-3} | Ext | 5ast,M |
| La2010b | ast5AL08cx | INPOP08a | 0.58 Myr | 5×10^{-3} | Ext | 5ast,M |
| La2010b* | ast5AL08cz | INPOP08a | 0.58 Myr | 4.8828125×10^{-3} | Ext | 5ast,M |
| La2010c | ast0AL08cx2a | INPOP08a | 1 Myr | 5×10^{-3} | Ext | 0ast,M |
| La2010c* | ast0AL08cz2a | INPOP08a | 1 Myr | 4.8828125×10^{-3} | Ext | 0ast,M |
| La2010d | ast5ALix | INPOP06 | 1 Myr | 5×10^{-3} | Ext | 5ast,M |

Note. The column "files" denotes the name of the computer files of the solution. "ephem" is the name of the reference INPOP ephemeris. "fit" is the time length of the ephemeris used for the fit. τ is the step size of the numerical integration. In "prec", Ext indicates that the integration was performed in extended precision. In the last column, 5ast indicates that 5 asteroids have been integrated, and M stands for the Moon as a separate object.

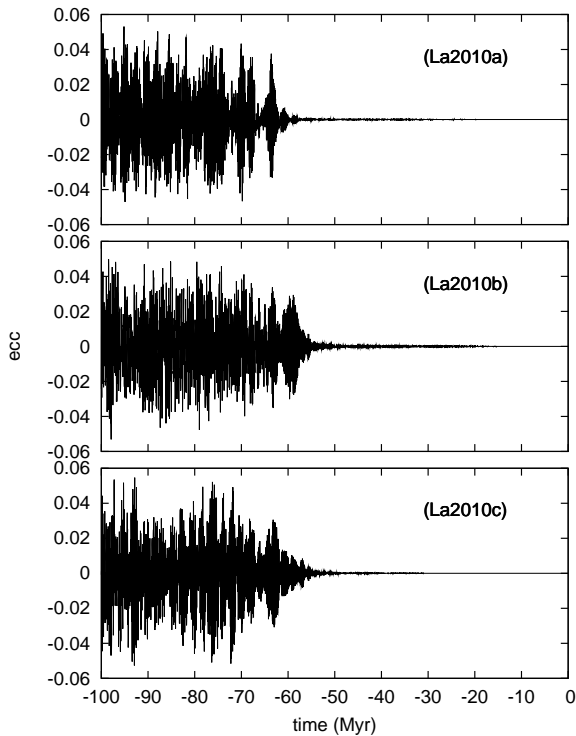


Fig. 1. Estimate of the numerical precision of the solutions La2010a,b,c. The estimate is obtained by the difference in the eccentricity of the Earth obtained with the integration of two solutions La2010x and La2010x* for $x = a, b, c$ (see Tab. 2).

of the initial conditions. In order to take into account the differences of models, we then perform a fit of the semi major axis, and add a small precessing term that can be thought as representative of the average contribution of the minor planets that have not been taken into account in our simplified models. In these solutions, the Moon is integrated as a separate object, taking into account the tidal dissipation in the Earth–Moon system. The step size is then 5×10^{-3} yr for La2010b,c,d and 10^{-3} yr for the nominal solution La2010a.

In order to check the numerical accuracy of the solution, we have also integrated these solutions with an alternate step size of $\tau^* = 4.8828125 \times 10^{-3}$ yr for b and c,

and $\tau^* = 0.9765625 \times 10^{-3}$ yr for La2010a*. These values are different, but close to the nominal step size. They are taken in such way that $1024 \times \tau^* = \tau$, where τ is the nominal step size of the corresponding solution. In Fig.1, the difference in the eccentricity of the Earth for two solutions La2010x and La2010x* are plotted over time for 100 Myr for $x = a, b, c$. Because of the exponential divergence of the solutions resulting from chaotic behavior, the difference is nearly zero for a very long time, of more than 50 Myr, and then grows rapidly to maximal value, as the two solutions will become out of phase.

This is an external way to evaluate the precision of the numerical integration, but it is in fact a pessimistic view. Indeed, we have fitted the solutions La2010a,b,c to INPOP08, but the initial conditions of La2010x* is the same as for La2010x. The difference of step size will then induce a difference of reference Hamiltonian in the symplectic integration of the system, which should explain most of the difference that is observed here. This is why for a reduced step size, as in La2010a, the difference between La2010a and La2010a* is smaller.

Nevertheless, although pessimistic, this shows that the numerical error can be neglected over 55 Myr for La2010b,c and 60 Myr for La2010a. This is why we have selected La2010a as our nominal solution.

5. Comparison with INPOP08

The solution La2004 was fitted to DE406 over its full range, that is over the interval $[-5000 : +1000]$ yr from now. In 2004, there was no possibility to compare it to an accurate ephemeris over a longer time. With the construction of the new INPOP ephemerides, this becomes now possible, as we have extended INPOP06 and INPOP08 over 1 Myr. As the set of observation used in INPOP08 is significantly larger than the one of INPOP06, we will use INPOP08 as the reference ephemeris, representing the best knowledge of the orbital motion of the Solar System that we can achieve at present.

We have thus compared La2004 to INPOP08 as well as INPOP06 and the new computed solutions of the Earth eccentricity for La2010a,b,c,d (Fig. 2). From Fig. 2 (top), it is clear that the new solution La2010a is a significant

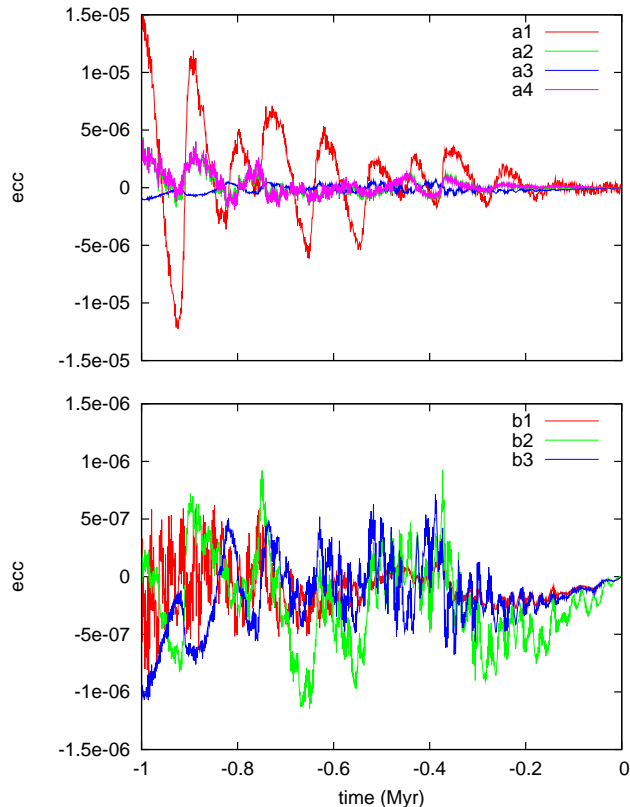


Fig. 2. Differences in the eccentricity of the Earth Moon barycenter over 1 Myr for various solutions as follows : a1 = La2004-INPOP08; a2 = La2010d-INPOP08; a3 = b3 = La2010a - INPOP08; a4 = INPOP06-INPOP08; b1 = La2010b - INPOP08; b2 = La2010c - INPOP06. It should be noted that the vertical scale is enlarged 10 times in the bottom plot. All solutions are compared to INPOP08. On the top figure, La2010d (a2) and INPOP06 (a4) are almost superposed. This is because La2010d was adjusted over INPOP06.

improvement with respect to La2004. Indeed, the difference La2010a-INPOP08 (Fig. 2 (a3) and (b3)) is nearly 15 times smaller than the difference La2004-INPOP08 (Fig. 2 (a1)).

In Fig. 2, we can see that La2010d-INPOP08 (a2) is almost superposed with INPOP06-INPOP08 (a4). This is because La2010d has been adjusted to INPOP06. It is also clear from this plot that the differences between a long time solution and its reference ephemeris are now much smaller than those of two consecutive versions of the high resolution planetary ephemeris (as INPOP06 and INPOP08).

The main result of these comparisons, are also displayed in Tables 3 and 4, for the various solutions that we have selected. The differences between the long term "simplified" model that we use here and the most precise planetary ephemerides are now much smaller than the difference

| | ast5AL08cx -INPOP08 1 Ma | | |
|---------|--------------------------|-----------------|-----------------|
| | $a \times 10^6$ | $e \times 10^6$ | $i \times 10^6$ |
| Mercury | 0.006 | 0.583 | 0.498 |
| Venus | 0.341 | 1.027 | 0.351 |
| EMB | 0.453 | 1.182 | 0.343 |
| Mars | 1.774 | 1.608 | 0.351 |
| Jupiter | 0.551 | 0.147 | 0.049 |
| Saturn | 1.758 | 0.359 | 0.037 |
| Uranus | 5.129 | 0.478 | 0.029 |
| Neptune | 8.734 | 0.306 | 0.027 |
| Pluto | 17.901 | 0.325 | 0.049 |
| Moon | 8.916 | 22005.375 | 12538.037 |
| | ast5SL08ax-INPOP08 1 Ma | | |
| | $a \times 10^6$ | $e \times 10^6$ | $i \times 10^6$ |
| Mercury | 0.002 | 3.962 | 2.859 |
| Venus | 0.155 | 1.975 | 0.978 |
| EMB | 0.224 | 1.540 | 0.968 |
| Mars | 1.744 | 2.823 | 0.954 |
| Jupiter | 0.278 | 0.113 | 0.033 |
| Saturn | 0.777 | 0.273 | 0.023 |
| Uranus | 2.256 | 0.352 | 0.020 |
| Neptune | 4.052 | 0.147 | 0.009 |
| Pluto | 8.805 | 0.165 | 0.019 |

Table 3. Maximum difference between the La2010 solutions and INPOP08 over 1 Myr. Top: Maximum difference ast5AL08cx -INPOP08 over 1 Myr. Bottom : Maximum difference ast5SL08ax -INPOP08 over 1 Myr. In ast5SL08ax, the Moon contribution is averaged. All solutions are in extended precision. EMB is the Earth-Moon barycenter. The semi-major axis a is in AU and the inclination with respect to the invariable plane i is in radians.

between two consecutive planetary ephemeris (INPOP06-INPOP08) that can be considered as representative of the true uncertainty of the ephemeris. The main limitation of the precision of the long term planetary solution then resides in the precision of the planetary ephemeris, that is in the planetary observations.

6. Comparison with La2004

After comparing the solutions over 1 Myr with the most precise planetary ephemeris, we will now compare the various solutions La2010a,b,c,d to the former solution La2004 over the whole expected range of validity of these solutions, that is over a few tens of million of years.

In (Fig.3), we have represented the variation of the eccentricity of the EMB from -30 Myr to -50 Myr for the La2004 solution and the four La2010a,b,c,d new solutions. The interval $[-30 : 0]$ Myr is not represented as all five solutions practically coincide over this time interval. Indeed, some discrepancies between La2004 and the new La2010 solutions only appear on the time interval $[-40 : -30]$, although most of the time the solutions are still very similar, and the small differences that can be seen on Fig.3 will most probably not lead to any significant change in the paleoclimate records. We can even consider that the solution La2004 is still in good agreement with the new solutions until -45 Myr. This is in good agreement with

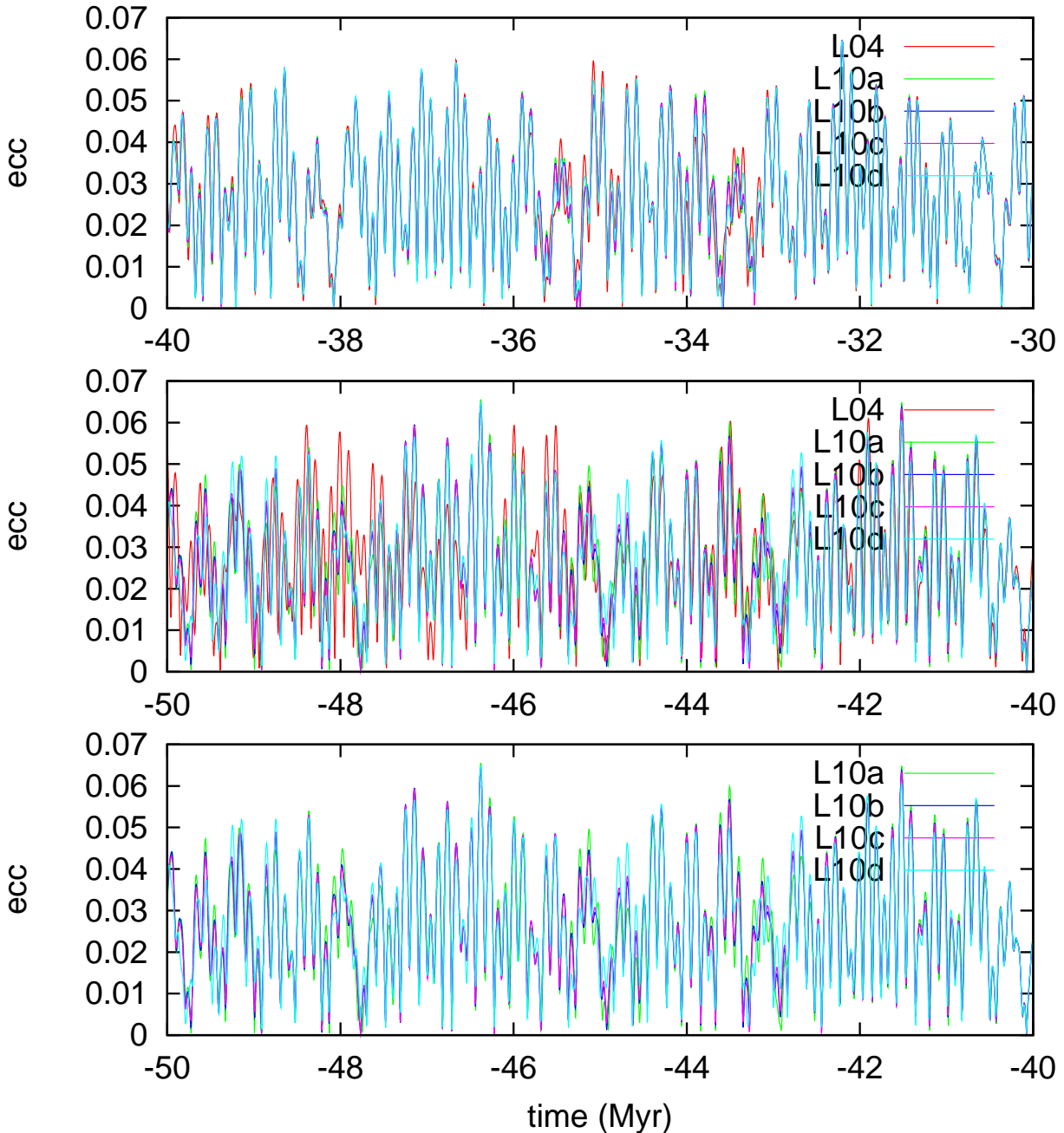


Fig. 3. Eccentricity of the Earth for the solutions La2004 (L04), La2010a (L10a), La2010b (L10b), La2010c (L10c), and La2010d (L10d). On the interval $[-40 : -30]$ Myr, the four solutions are virtually identical, but before -45 Myr, La2004 begins to depart significantly from the La2010 solutions. We have then plotted again the time interval $[-50 : -40]$ Myr (bottom), removing La2004 for a better comparison of the La2010 solutions. Over this interval, these three solutions are very similar.

the expected precision that was forecasted in (Laskar et al. 2004).

Beyond -45 Myr, noticeable differences become to appear, and the solution La2004 becomes significantly different than the La2010 solutions. We have thus made an additional plot of the $[-50 : -40]$ Myr interval on Fig.3, with only the solutions La2010a,b,c,d. These latest solutions well agree on this time interval, despite the variations of models or initial conditions among these new solutions.

We can thus consider that the present new solutions are at least valid over 50 Myr.

Beyond -50 Myr, the situation is more confused as the solutions La2010a,b,c,d present significant variations (Fig. 4). Nevertheless, from Fig. 4, it can be seen that if moderate precision is only required, the solution could eventually used up to -60 Myr. In particular, the solutions are still well in phase around -55 Myr. This date is of particular interest, as it corresponds to specific climatic events that have been well documented in the paleoclimate records :

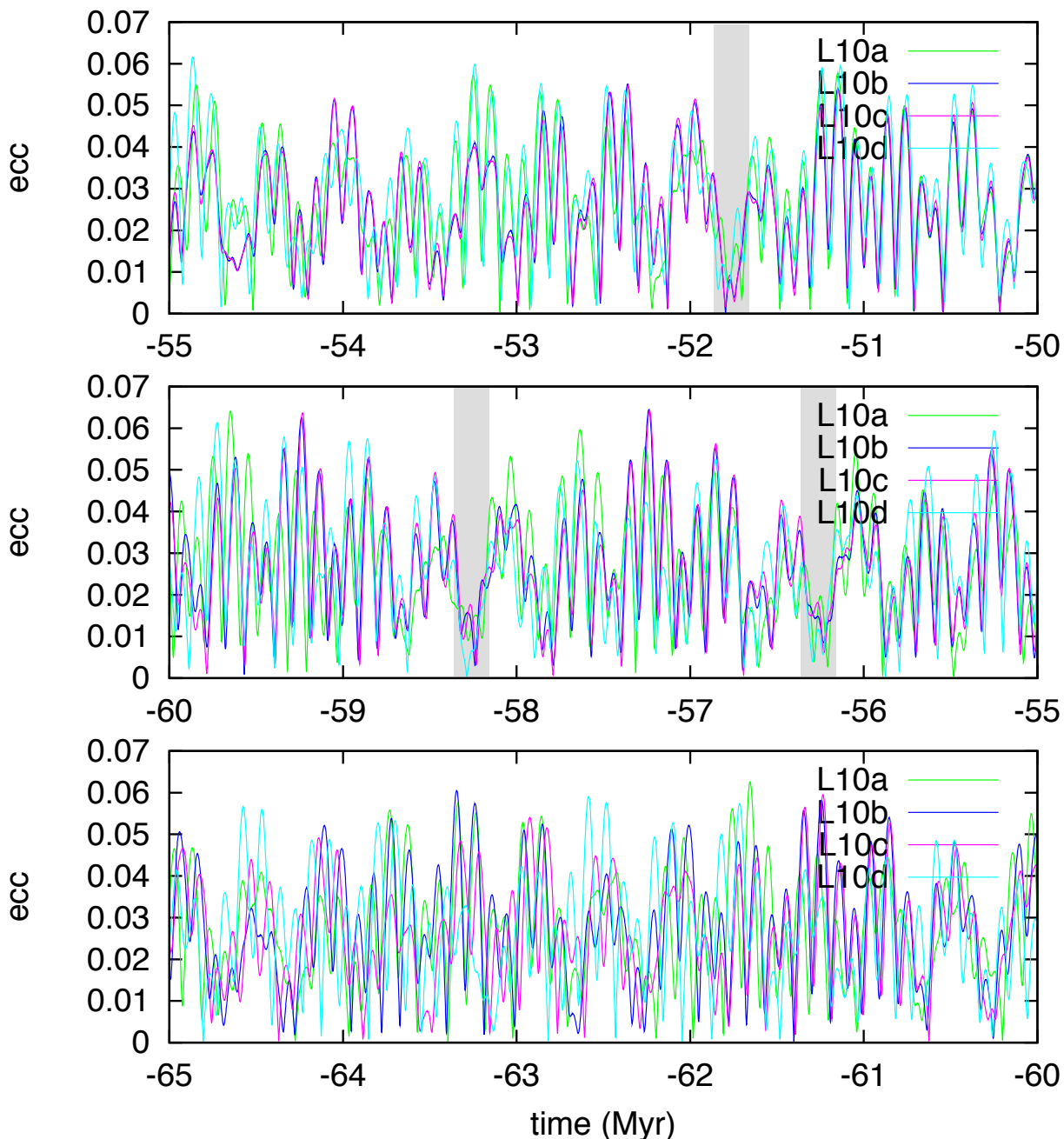


Fig. 4. Eccentricity of the Earth for the solutions La2010a (L10a), La2010b (L10b), La2010c (L10c), and La2010d (L10d) from -50 to -65 Myr. Although the various solution begin to diverge beyond 53 Ma, it is remarkable that the minima of eccentricity at 51.75 Ma, 56.25 Ma and 58.25 Ma (in grey) correspond in all various solutions.

the Paleocene-Eocene Thermal Maximum (PETM) that is dated around 55.53–56.33 Ma¹ (Westerhold et al. 2007, 2008), and the Elmo Thermal Maximum (ETM) dated at 53.7–54.5 Ma (Lourens et al. 2005; Westerhold et al. 2007, 2008).

On the other hand, from Fig. 4, it is quite clear that the solutions La2010a,b,c,d cannot be used beyond 60

Ma, as the solutions have large differences in the interval $[-65 : -60]$ Myr. It should thus be stressed that in this time interval, the direct use of the eccentricity solution of the Earth for geological calibration should be used with utmost care.

Practically, if one wishes to use these solutions beyond 50 Myr, for a geological calibration for example, one should use only the features of the solutions that remain the same in the four La2010 solutions. This will assess the

¹ Myr design the duration of 1 million of years, while Ma stands for mega-annum, and represent date in the past from the present.

| ast5ALix -INPOP06 1 Ma | | | |
|------------------------|-----------------|-----------------|-----------------|
| | $a \times 10^6$ | $e \times 10^6$ | $i \times 10^6$ |
| Mercury | 0.005 | 0.473 | 0.342 |
| Venus | 0.034 | 0.503 | 0.209 |
| EMB | 0.049 | 0.505 | 0.234 |
| Mars | 0.721 | 0.873 | 0.397 |
| Jupiter | 0.121 | 0.069 | 0.046 |
| Saturn | 0.980 | 0.157 | 0.032 |
| Uranus | 1.553 | 0.139 | 0.025 |
| Neptune | 2.263 | 0.068 | 0.020 |
| Pluto | 7.068 | 0.104 | 0.022 |
| Moon | 21.439 | 26686.705 | 12769.784 |
| ast5ALh-INPOP08 1 Ma | | | |
| | $a \times 10^6$ | $e \times 10^6$ | $i \times 10^6$ |
| Mercury | 0.007 | 0.503 | 0.357 |
| Venus | 0.290 | 1.156 | 0.225 |
| EMB | 0.379 | 0.986 | 0.257 |
| Mars | 2.757 | 2.484 | 0.469 |
| Jupiter | 0.563 | 0.139 | 0.047 |
| Saturn | 2.406 | 0.272 | 0.034 |
| Uranus | 5.415 | 0.268 | 0.026 |
| Neptune | 9.845 | 0.320 | 0.021 |
| Pluto | 19.768 | 0.361 | 0.052 |
| Moon | 21.093 | 26481.398 | 12727.162 |

Table 4. Maximum difference between the La2010 solutions and INPOP06 over 1 Myr. Top: Maximum difference ast5ALix-INPOP06 (Both solutions are in extended precision) over 1 Myr. Bottom: Maximum difference ast5ALh-INPOP06 over 1 Myr. The solution ast5ALh has been computed in double precision, while INPOP06 is in extended precision. Both solutions have been fitted to INPOP06 over 1 Myr. EMB is the Earth-Moon barycenter. The semi-major axis a is in AU and the inclination with respect to the invariable plane i is in radians.

Table 5. Frequency decomposition of $z = e \exp i\varpi$ for the Earth on the time interval $[-15, +5]$ Myr (Laskar *et al.*, 2004).

| n | μ_k (°/yr) | b_k | φ_k (degree) | |
|-----|----------------|-----------|----------------------|----------|
| 1 | g_5 | 4.257564 | 0.018986 | 30.739 |
| 2 | g_2 | 7.456665 | 0.016354 | -157.801 |
| 3 | g_4 | 17.910194 | 0.013055 | 140.577 |
| 4 | g_3 | 17.366595 | 0.008849 | -55.885 |
| 5 | g_1 | 5.579378 | 0.004248 | 77.107 |

stability of such a calibration with respect to the uncertainty of the La2010 solutions.

7. Long term cycles

The complete eccentricity solution of the Earth allow a direct adjustment of paleoclimate data to the oscillations of about 95 kyr and 124 kyr of the eccentricity (see Laskar *et al.* 2004), but for ancient records, this signal may not be clearly visible in the sediments. On the other way, the 405 kyr oscillation with argument $g_2 - g_5$, where g_i (Table 6) are the secular frequencies of the Solar System (see Laskar *et al.* 2004) is very often present in the sedimentary records. This term is the largest term in a quasi periodic approximation of the eccentricity of the Earth

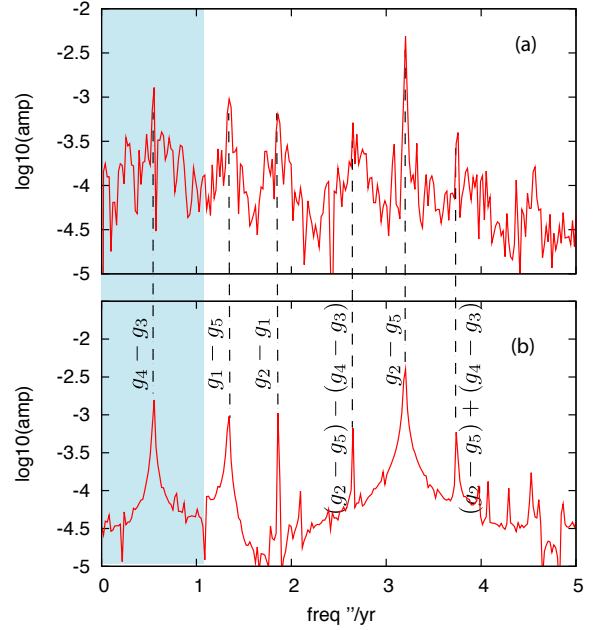


Fig. 5. In (a) is the spectrum of the eccentricity over 65Myr from the La2010a solution, limited to the interval $[0, 5''/yr]$. In (b), the same spectrum is plotted for a solution build with only the 5 main terms of z_3 (Table 5). The main peaks are then easily identified and thus also the main peaks of the full eccentricity (a).

Table 6. Main secular frequencies g_i and s_i of La2004 and La2010a determined over 20 Ma for the four inner planets, and over 50 Ma for the 5 outer planets (in arcsec yr⁻¹). Δ_{100} are the observed variations of the frequencies over 100 Myr (Laskar *et al.* 2004). In the last column, the period of the secular term are given.

| | La2004 | La2010a | Δ_{100} | period (yr) |
|-------|------------|------------|----------------|-------------|
| g_1 | 5.59 | 5.59 | 0.13 | 231 843 |
| g_2 | 7.452 | 7.453 | 0.019 | 173 913 |
| g_3 | 17.368 | 17.368 | 0.20 | 74 620 |
| g_4 | 17.916 | 17.916 | 0.20 | 72 338 |
| g_5 | 4.257452 | 4.257482 | 0.000030 | 304 407 |
| g_6 | 28.2450 | 28.2449 | 0.0010 | 45 884 |
| g_7 | 3.087951 | 3.087946 | 0.000034 | 419 696 |
| g_8 | 0.673021 | 0.673019 | 0.000015 | 1 925 646 |
| g_9 | -0.34994 | -0.35007 | 0.00063 | 3 703 492 |
| s_1 | -5.59 | -5.61 | 0.15 | 231 843 |
| s_2 | -7.05 | -7.06 | 0.19 | 183 830 |
| s_3 | -18.850 | -18.848 | 0.066 | 68 753 |
| s_4 | -17.755 | -17.751 | 0.064 | 72 994 |
| s_5 | | | | |
| s_6 | -26.347855 | -26.347841 | 0.000076 | 49 188 |
| s_7 | -2.9925259 | -2.9925258 | 0.000025 | 433 079 |
| s_8 | -0.691736 | -0.691740 | 0.000010 | 1 873 547 |
| s_9 | -0.34998 | -0.35000 | 0.00051 | 3 703 069 |

(see Laskar *et al.* 2004, Table 6), and is less influenced by the chaotic diffusion present in the Solar system than the shorter period terms around 100 kyr (Laskar 1990; Laskar *et al.* 2004).

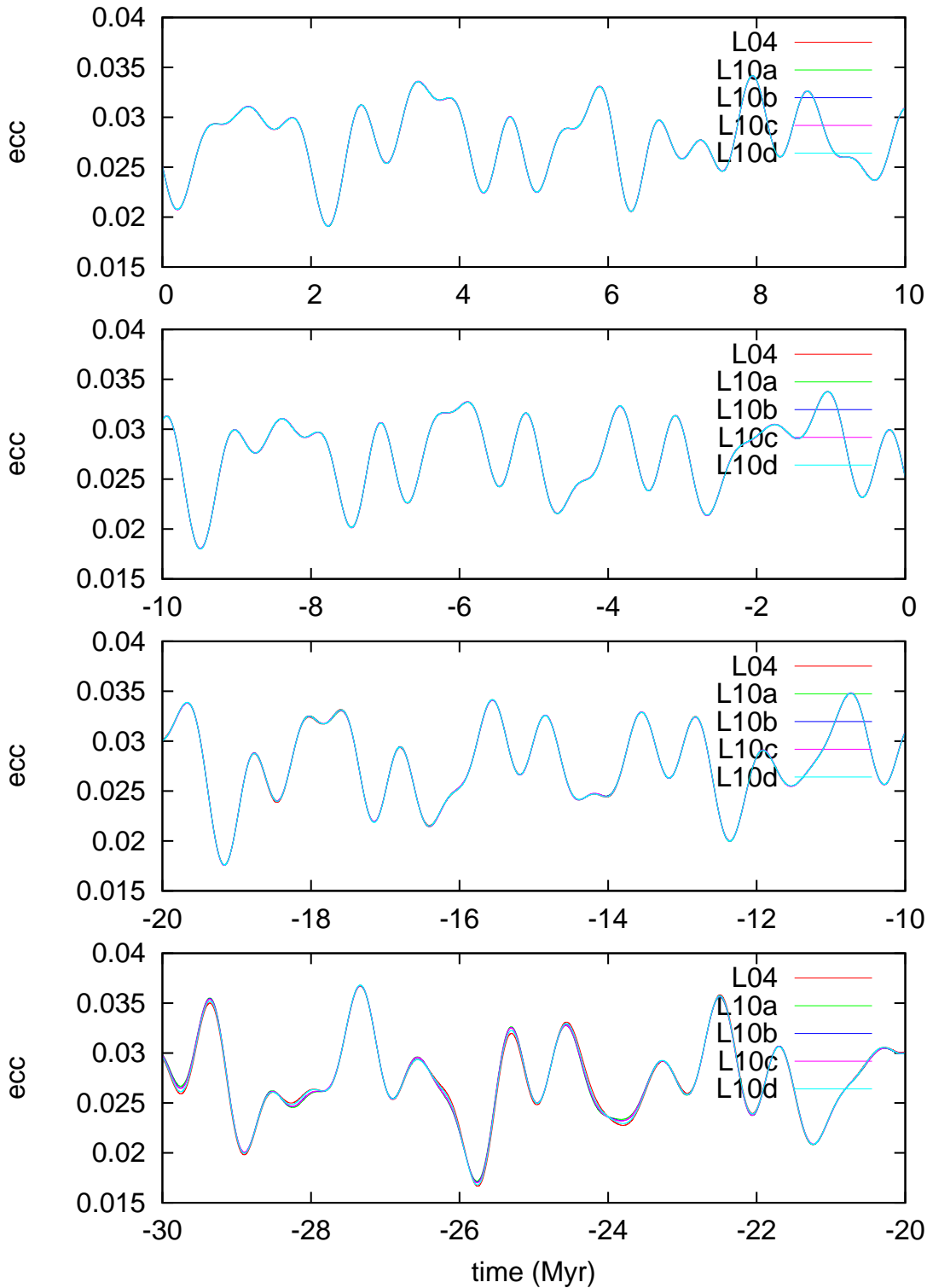


Fig. 6. Filtered eccentricity of the Earth for the solutions La2004 (L04), La2010a (L10a), La2010b (L10b), La2010c (L10c), and La2010d (L10d) from +10 to -30 Myr. The solution is filtered in the interval $[0 : 2.2''/\text{yr}]$, that is for periods in $[589, +\infty[$ kyr.

In recent works, the modulation of the 405 kyr component, due to the beat $g_3 - g_4$ of period ≈ 2.4 Myr has also been identified in the sedimentary records, and is thought to be a key factor for the onset of special climate events (Lourens *et al.* 2005; Pälike *et al.* 2006; van Dam *et al.*

2006). More generally, there has been a large effort to search for long term cycles in the sedimentary records and to use them to hook the sedimentary data to the eccentricity computations (Olsen & Kent 1996; Lourens *et al.* 2005; Westerhold *et al.* 2007, 2008; Jovane *et al.* 2010).

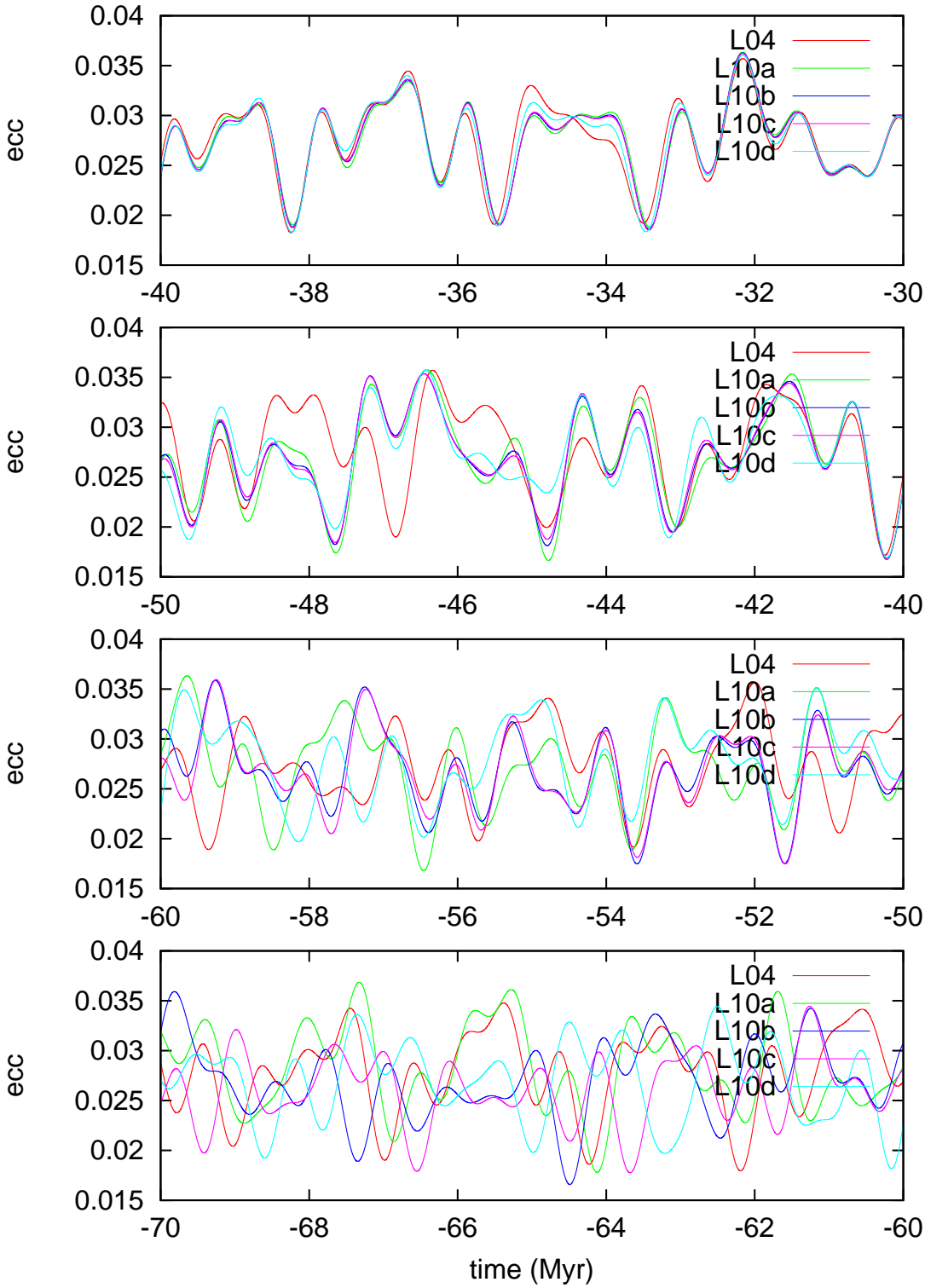


Fig. 7. Filtered eccentricity of the Earth for the solutions La2004 (L04), La2010a (L10a), La2010b (L10b), La2010c (L10c), and La2010d (L10d) from -30 to -70 Myr. The solution is filtered in the interval $[0 : 2.2''/\text{yr}]$, that is for periods in $[589, +\infty[$ kyr.

In figure 5a is plotted the spectrum of the nominal solution La2010a, limited to the range $[0, 5]''/\text{yr}$ (periods larger than 260 kyr). As there is a gap at about $2.2''/\text{yr}$ in this spectrum, we have filtered the eccentricity data for

all various solutions in the range $[0, 2.2]''/\text{yr}$ (Figures 6, 7).

Here again, it is clear that all solutions La2004, and La2010a,b,c,d are practically identical over $[-30 : 0]$ Myr, and very similar up to -45 Myr, where La2004 starts to

differ notably from the new solutions La2010, which still behave in a similar manner up to about -50 Myr where the situation becomes more confused.

7.1. The modulation of the $g_2 - g_5$ 405 kyr cycle

In order to examine more closely the long term cycles in the Earth eccentricity, we have identified the origin of the main spectral terms in the eccentricity spectrum of figure 5a. In order to do so, a synthetic eccentricity curve is build along the same time range using only the five terms of $e \exp(i\varpi)$, as provided by the frequency decomposition of the solution La2004 over the time interval $[-15, +5]$ Myr, taken from (Laskar *et al.* 2004). The plot of the spectrum of the eccentricity function that is obtained with this purely quasiperiodic signal with frequencies limited to the linear terms g_1, g_2, g_3, g_4, g_5 (Table 5) is plotted in Figure 5b.

As this synthetic model is quasiperiodic with only five main frequencies, the identification of the main spectral terms of the eccentricity are then obtained unambiguously with a spectral analysis over 65 Myr and are detailed in figure 5b. These terms are easily related to the corresponding peaks of the full eccentricity spectrum of Figure 5a.

This exercise, that is in some sense complementary from a full quasiperiodic decomposition of the eccentricity as in (Laskar *et al.* 2004, Table 6) allows to better understand the behavior and origin of the main long term cycles observed by the practitioners when comparing to geological data (Olsen & Kent 1996; Lourens *et al.* 2005; Westerhold *et al.* 2007, 2008; Jovane *et al.* 2010; Hilgen *et al.* 2010).

The leading periodic term is the well known 405 kyr term $g_2 - g_5$, but this term is surrounded by two terms $(g_2 - g_5) - (g_4 - g_3)$ and $(g_2 - g_5) + (g_4 - g_3)$ that will induce with $g_2 - g_5$ a modulation of the 405 kyr eccentricity term with a frequency of $g_4 - g_3$, corresponding to a 2.4 Myr period. An obvious consequence is that when analyzing geological data to search for the 405 kyr term, one needs to use a spectral window that includes these two side terms, that is a window similar to the $[2.2, 4.3]$ "/yr window used in figure 8. Additionally, the two terms $g_1 - g_5$ of period ≈ 1 Myr, and $g_2 - g_1$ of period ≈ 688 kyr are also of strong amplitude in the eccentricity spectrum.

7.2. The $g_4 - g_3$ 2.4 Myr cycle

Moreover, $g_4 - g_3$ appears also directly as a main periodic term of the eccentricity (Fig.5a,b). The same 2.4 Myr cycle can thus be directly retrieved from the eccentricity curve. Indeed, in figure 8, we have plotted both the filtered eccentricity in the interval $[2.2, 4.3]$ "/yr (e^a) (in red) and as well the filtered eccentricity with a $[0, 0.1]$ "/yr window (e^b) (in blue). It can then be seen that the envelope (in green) of e^a is almost identical to the opposite of e^b (Fig. 8).

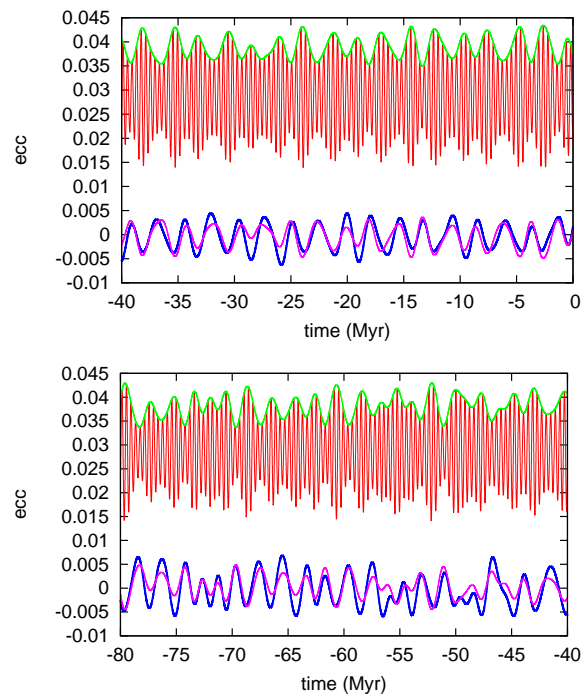


Fig. 8. Filtered eccentricity around the 405 kyr period for La2010a. In red is e^a , the filtered eccentricity in the band $[2.2, 4.3]$ "/yr ($[301, 589]$ kyr period), while e^b , the filtered eccentricity in the band $[0, 0.1]$ "/yr (period > 1.18 Myr) is plotted in blue. The opposite (in pink) of the maximum envelope of e^a (in green) nearly coincide with e^b .

As a consequence, the two components e^a and e^b of the eccentricity need to be added in order to really evaluate the component of the 2.4 Myr term (Fig. 9). In the resulting $e^a + e^b$ curve, the variation of the maxima are then attenuated while the minima variations are increased to about 0.02. The variations of the minima are in phase with the $g_4 - g_3$ term (plotted in blue in Fig. 9).

The large size of these variations makes it then understandable that a signature of these variations could be recorded in the sedimentary paleoclimate signal. Indeed, although the global mean annual insolation on earth varies as e^2 and thus is not much influenced by eccentricity variations, this is not the case for seasonal variations. Indeed, if one considers a black body with uniform temperature at distance d of a star, using Stefan's law for the emission of a black body, one finds that its surface temperature T is proportional to $d^{-1/2}$. In this case, the difference δT between perihelion and aphelion temperature will be given by

$$\frac{\delta T}{T} \approx \frac{1}{2} \frac{2ae}{a} = e. \quad (1)$$

A change of 0.02 in the eccentricity corresponds thus in this simplify model to a change of about $0.02 \times 300 = 6$ K in the difference between perihelion and aphelion temperatures.

Because of the increasing importance of this 2.4 Myr component in some of the analysis of sedimentary records,

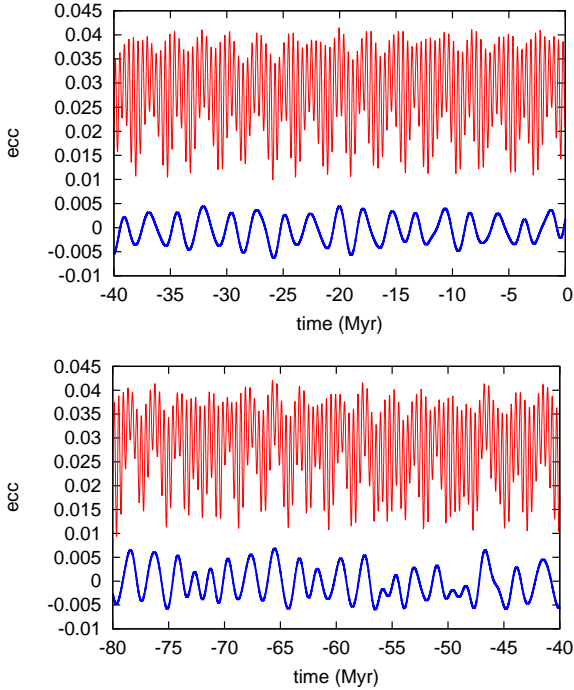


Fig. 9. $e^a + e^b$ (see Fig. 8) for the La2010a solution is plotted in red. Its minimum are in phase with e^b , the filtered eccentricity in the band $[0, 1.1]''/\text{yr}$ (in blue).

we have added here a detailed comparison of the filtered solution in the $[0, 1.1]''/\text{yr}$ interval in figure 10 for the time intervals $[-55, -40]$ and $[-65, -50]$ Myr time intervals. It should be noted that it is not necessary to compare the various orbital solutions in the $[-40, 0]$ Myr time interval as they are practically identical in this range.

As in the previous discussion, we can see that all curves are very similar until -45 Myr, while La2004 differs significantly beyond -45 Myr. This is why this solution is no longer plotted on the bottom plot of figure 10, which is displayed on the $[-65, -50]$ time interval. This range is particularly critical, as it corresponds both to the location of the PETM (at about -55 Myr) and of the K/P boundary (at about -66 Myr) (Lourens *et al.* 2005; Westerhold *et al.* 2007, 2008). The various solutions begin to differ significantly beyond -53 Myr, but it can be remarked that the two maxima at about -57.3 Myr and -59.3 Myr agree for all four La2010 solutions, although they largely differ around -55 Myr. One could thus use these three peaks in order to attempt to fit a geological time scale beyond -50 Myr, in the $[-60, -50]$ Myr interval.

In fact, in the La2010a solution, the $g_4 - g_3$ argument has a period of about $2\pi/2.664 \approx 2.36$ Myr in the interval $[-45, 0]$ Myr, but beyond -45 Myr, this period changes due to chaotic diffusion (Fig. 11). As this occurs at the border of the validity range of the solution, it is still difficult to be sure of the real behavior of the $g_4 - g_3$ argument beyond -45 Myr, and it will be necessary to confront these data to geological records to confirm the behavior of the solar system eccentricity solution.

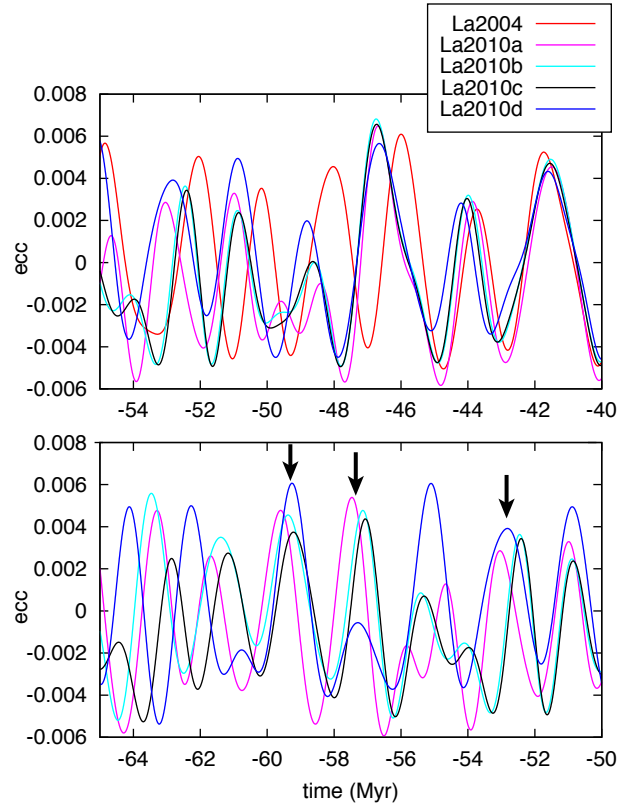


Fig. 10. Filtered eccentricity in the band $[0, 1.1]''/\text{yr}$ (period > 1.18 Myr) for La2004 and La2010a,b,c,d.

8. Resonant angles

8.1. Secular resonances

The previous discussion demonstrates the importance of the behavior of the $g_4 - g_3$ argument in the macroscopic aspect of the variations of the Earth's eccentricity, and thus its possible relation with the past climate on Earth.

Indeed, using the secular equations, Laskar (1990, 1992) demonstrated that the chaotic behavior of the Solar System arise from multiple secular resonances in the inner Solar System, and in particular, from the critical argument associated to

$$\theta = (s_4 - s_3) - 2(g_4 - g_3) \quad (2)$$

where g_3, g_4 are related to the precession of the perihelion of the Earth and Mars, s_3, s_4 are related to the precession of the node of the same planets. This argument is presently in a librational state, but can evolve in a rotational state, and even move to libration in a new resonance, namely

$$(s_4 - s_3) - (g_4 - g_3) = 0. \quad (3)$$

The argument θ as well as the other important resonant argument ($\sigma = (g_1 - g_5) - (s_1 - s_2)$) that was identified by Laskar (1990, 1992) as the origin of the chaotic behavior of the inner planets are plotted in figure 12 for all solutions La2004, La2010a,b,c,d. In all cases, transition from libration to circulation appear around -50 Myr, leaving

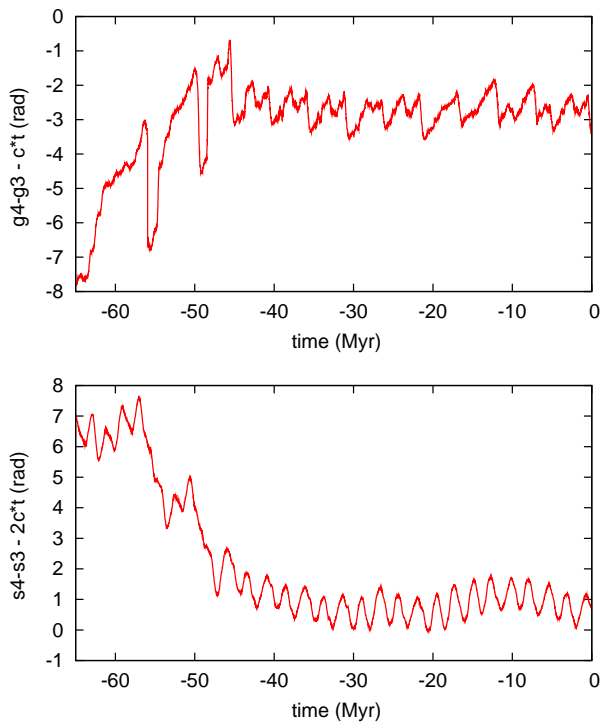


Fig. 11. Argument (in radians) related to $g_4 - g_3 - 2.664T$ versus T (in Myr) for La2010a (top). Argument (in radians) related to $s_4 - s_3 - 2 \times 2.664T$ versus T (in Myr) for La2010a (bottom).

some uncertainty to the behavior of the solution beyond this date.

8.2. Searching for some geological evidence of chaos

The transition from libration to circulation of the resonant argument related to $\theta = (s_4 - s_3) - 2(g_4 - g_3)$ is directly linked with the chaotic diffusion of the orbital trajectories. Searching in the geological record for the evidence of such a transition would thus be an observational confirmation of the past evolution of the Solar System.

As it appears in the previous sections, it becomes more and more difficult to obtain by numerical computations only the date of the first transition from libration to circulation for this resonant argument (Fig. 12). The direct observation of the individual arguments related to g_3, g_4, s_3, s_4 is certainly out of reach. On the other hand, the argument θ corresponds to a 2 : 1 resonance between the two secular terms $g_4 - g_3$ and $s_4 - s_3$, both terms being present in the sedimentary records. We have discussed about the importance of the $g_4 - g_3$ beat in the eccentricity solution. In a similar way, $s_4 - s_3$ appears as a beat of about 1.2 million of years in the solution of obliquity, as the result of the beat between the $p + s_4$ and $p + s_3$ components of the obliquity, where p is the precession frequency of the axis (see Laskar *et al.* 2004, Fig. 7).

With the occurrence of these beats, the detection of the resonant state in the geological data becomes possible. Indeed, the modulation of 1.2 Myr of the obliquity

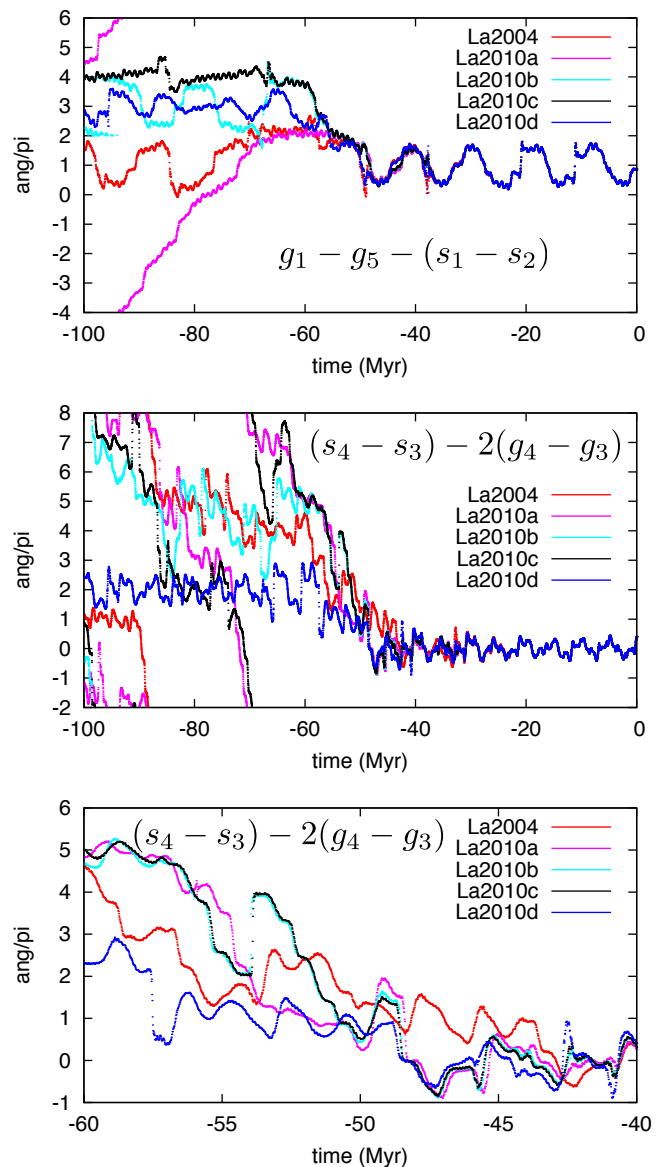


Fig. 12. Resonant arguments (in radians versus time in Myr) $\sigma = (g_1 - g_5) - (s_1 - s_2)$ (top) and $\theta = (s_4 - s_3) - 2(g_4 - g_3)$ (middle and bottom) for the different solutions La2004, La2010a,b,c,d. In the bottom plot, θ is displayed at a greater scale. One can see that the La2010 solutions are very close up to 50 Myr.

appears clearly in the spectral analysis of the paleoclimate record from Ocean Drilling Program Site 926, (Zachos *et al.* 2001). Moreover, using the ODP legs 154 and 199, Pälike *et al.* (2004) could find some evidence that the critical argument of θ did not show a transition to circulation at 25 Myr, as in La93, but remained in libration over 30 Myr, as in the La2004 solution.

Searching for a transition of the $(s_4 - s_3) - 2(g_4 - g_3)$ resonance to the $(s_4 - s_3) - (g_4 - g_3)$ resonance, as displayed in figure 12) is difficult, as it requires to obtain both a good signal in eccentricity (or precession) and in obliquity. It may be more direct to search only for a modulation of the $g_4 - g_3$ (or $s_4 - s_3$) period, as it appears in figure 11.

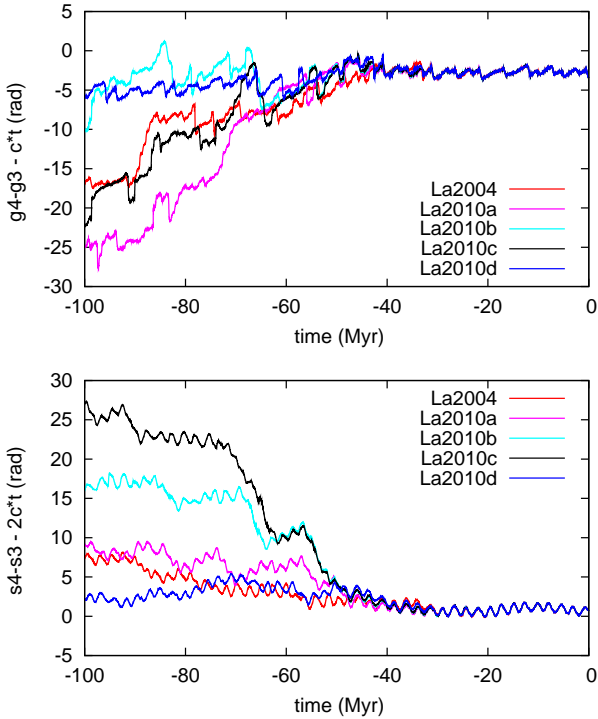


Fig. 13. Argument (in radians) related to $g_4 - g_3 - 2.664T$ versus T (in Myr) for various orbital solutions (top). Argument (in radians) related to $s_4 - s_3 - 2 \times 2.664T$ versus T (in Myr) for various orbital solutions (bottom).

Indeed, the change in La2010a at -45 Myr of the $g_4 - g_3$ slope, from a period of about 2.4 Myr to a period of about 2 Myr also reflects the same chaotic transition.

In fact, this change can be directly seen in the eccentricity record (Figs 9, 10), as it will induce a change of the time interval from two maxima in the filtered eccentricity (Figs 10) from a 2.4 Myr period to a 2 Myr period. If the 405 kyr $g_2 - g_5$ signal is well present in the geological data, this becomes then a macroscopic feature that can be detectable. Indeed, a local time scale can be established using the 405 kyr signal, and the modulation period of this signal should be the $g_4 - g_3$ term. The transition is then obtained as a transition from 6 periods per beat to 5 periods per beats. Such geological data could then be able to discriminate among the various La2010 solutions (Fig. 13). It becomes therefore even more important to search for good sedimentary sections where the 405 kyr signal is well determined.

9. Stability of the $g_2 - g_5$ 405 kyr cycle

As it was stressed above, the $g_2 - g_5$ 405 kyr argument has a particular importance in long time geological calibration, as it is present in many sedimentary records and its good stability (Laskar 1990) can allow to use it as a reference time scale. This argument is indeed visible in many sedimentary records of the Early Mesozoic (Olsen & Kent 1999, and references therein). As in (Laskar et al. 2004), we have tested the stability of this argument over the full

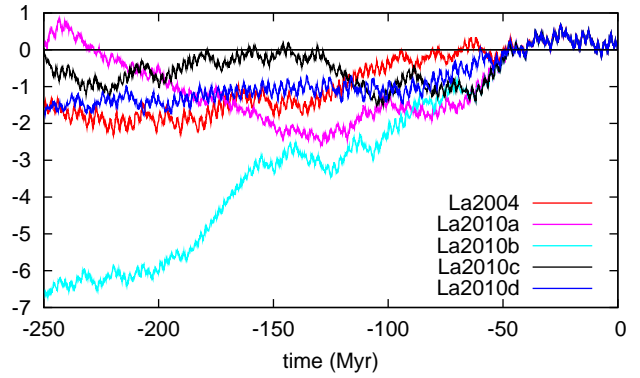


Fig. 14. 405 kyr term in eccentricity. Maximum difference (in radians) of the argument $\theta_{g_2-g_5}(t) - \theta_{g_2-g_5}(0)$ of $g_2 - g_5$ in all solutions La2004, La2010a,b,c,d with respect to the linear approximation $\theta_0(t) = 3.200''t$ where t is in yr.

period of our integrations, that is over 250 Myr by comparison of its evolution on all retained La2010 solutions and La2004 (14). The present values of $g_2 - g_5$ do not differ significantly from the value of La2004 (Laskar et al. 2004). The frequency $g_2 - g_5$ is thus kept to its La2004 value

$$\nu_{405} = 3.200''/\text{yr} \quad (4)$$

which corresponds exactly to a period

$$P_{405} = 405000 \text{ yr.} \quad (5)$$

As seen in Fig 14, the maximum deviation obtained by comparing all solutions is about 2π over 250 Myr, which correspond to a full cycle of 405 kyr after 250 Myr, as was given already in (Laskar et al. 2004).

10. Discussion and future work

The new orbital solutions of the Earth that are presented here can be used for paleoclimate computations over 50 Myr. Beyond that time interval, the precision of the solution cannot be guaranteed but we nevertheless provide the solution over 250 Myr on our Web site www.imcce.fr/Equipes/ASD/insola/earth/earth.html as reference, and for a possible use, with caution, over the full Paleogene period (up to 65 Myr).

In order to allow practitioners to test the stability of the solution and deduced calibration, we have decided to provide the four solutions that have been discussed here, La2010a,b,c,d, La2010a being the nominal solution.

It should be stressed that La2010a is chosen as the nominal solution because of its better numerical accuracy, but there is no strong clue that La2010a should behave better than the other ones. Before -50 Myr, they behave practically all in the same way. beyond -50 Myr, the robustness of a fit could be tested by changing the solutions. Alternatively, in presence of convincing geological record, one may conclude that one solution is more probable than another one. This will be in some sense a feedback from geology to celestial mechanics.

Contrary to (Laskar et al. 1993a) and (Laskar et al. 2004), we have provided here only the eccentricity solution. Indeed, although the model for the Earth rotational evolution has been improved, the main uncertainty linked to the evolution of the tidal dissipative effect in the past is still the main unknown parameter for the precession and obliquity evolution, and we thus do not believe that a new solution would provide more insight than La2004, unless a full analysis of the geophysical effects is made, in confrontation with the geological records, which becomes then out of the scope of the present paper. We thus refer to La2004 for precession and obliquity.

On the other hand, we plan to release soon a full high precision, non averaged solution of the rotation and precession of the Earth over 1 Myr, as computed from the INPOP model.

After the publication of the La2004 solution (Laskar et al. 2004), our goal was to search for an improved solution, valid over the full cenozoic era. We must say that we have not reached this goal. Although the present solution presents a significant improvement with respect to La2004, it is only valid over about 50 Myr.

The main improvement in the present solution was to use a 1 Myr version of the INPOP ephemeris (Fienga et al. 2008, 2009) in order to fit the initial conditions and parameters of the model. As future versions of INPOP will appear (Fienga et al. 2010), we will be able to better evaluate the real accuracy of our model.

At this point, it is still difficult to say whether it will be possible to obtain a precise solution over 65 Myr for the eccentricity of the Earth. Indeed, in the present solution, we have used a more complex model, by adding the five main asteroids in the orbital computation, but this added also some instabilities in the system, and although we increased the numerical accuracy of the algorithm by using extended precision instead of double precision, we did not reach a better numerical accuracy than in La2004. We intend to improve on this point, and to increase the numerical accuracy of the solution, as we would like to be sure that the numerical precision is not the limiting factor in the final precision of the solution. In order to do so, we will also need to improve at the same time on the speed of the algorithm, as the present version of our nominal solution La2010a took nearly 18 months to complete.

With the present solution (La2010), we have reached the limit of the observational data, and the limit of predictability for a precise solution of the orbital evolution of the Earth. We have thus decided to provide several possible outcomes instead of a single one as usual. The solutions La2010a,b,c,d are all available on the Web site www.imcce.fr/Equipes/ASD/insola/earth/earth.html.

Practitioners can thus check which of these solutions best fit their data beyond -50 Myr. Moreover, it becomes clear that the long periodic terms related to $g_4 - g_3$ in the eccentricity, that appears also as modulation of the the 405 kyr term in the eccentricity, and the equivalent $s_4 - s_3$ term in the inclination, are some key macroscopic features of the orbital solution that are imprinted in the geological

record. Their precise recovery can thus provide some clue for the past chaotic diffusion of the orbital motion of the Earth.

Acknowledgements. This work was supported by ANR-ASTCM. It benefited from support from INSU-CNRS, PNP-CNRS, and CS, Paris Observatory.

References

- Bills, B. G. 1994, *Geophysical Research Letters*, 21, 177
 Boué, G. & Laskar, J. 2006, *Icarus*, 185, 312
 Chapman, S. & Lindzen, R. S. 1970, *Atmospheric Tides*
 Correia, A. C. M. & Laskar, J. 2003, *Icarus*, 163, 24
 Correia, A. C. M., Laskar, J., & de Surgy, O. N. 2003, *Icarus*, 163, 1
 Darwin, G. H. 1880, *Philos.Trans.R.Soc.London*, 171, 713
 Fienga, A., Laskar, J., Morley, T., et al. 2009, *Astronomy and Astrophysics*, 507, 1675
 Fienga, A., Manche, H., Kuchynka, P., Laskar, J., & Gastineau, M. 2010, *Planetary and Lunar ephemerides, INPOP10A*, arXiv:1011.4419v1
 Fienga, A., Manche, H., Laskar, J., & Gastineau, M. 2008, *Astronomy and Astrophysics*, 477, 315
 Folkner, W. M. 2008, 343R, 8
 Forte, A. M. & Mitrovića, J. X. 1997, *Nature*, 390, 676
 Gradstein, F. M., Ogg, J. G., & Smith, A. G. 2004, *A Geological Time Scale 2004*, 589, cited By (since 1996): 1291
 Hays, J. D., Imbrie, J., & Shackleton, N. J. 1976, *Science*, 194, 1121
 Hilgen, F., Kuiper, K., & Lourens, L. 2010, *Earth and Planetary Science Letters*, 300, 139
 Ito, T., Masuda, K., Hamano, Y., & Matsui, T. 1995, *Journal of Geophysical Research*, 100
 Jovane, L., Sprovieri, M., Coccioni, R., et al. 2010, *Earth and Planetary Science Letters*, 298, 77
 Laskar, J. 1988, *Astronomy and Astrophysics*, 198, 341
 Laskar, J. 1989, *Nature*, 338, 237
 Laskar, J. 1990, *Icarus*, 88, 266
 Laskar, J. 1992, *IAU Symp.*, 1, 152
 Laskar, J. 1999, *Royal Society of London Philosophical Transactions Series A*, 357, 1735
 Laskar, J. & Gastineau, M. 2009, *Nature*, 459, 817
 Laskar, J., Joutel, F., & Boudin, F. 1993a, *Astronomy and Astrophysics*, 270, 522
 Laskar, J., Joutel, F., & Robutel, P. 1993b, *Nature*, 361, 615
 Laskar, J., Quinn, T., & Tremaine, S. 1992, *Icarus*, 95, 148
 Laskar, J. & Robutel, P. 2001, *Celestial Mechanics and Dynamical Astronomy*, 80, 39
 Laskar, J., Robutel, P., Joutel, F., et al. 2004, *Astronomy and Astrophysics*, 428, 261
 Levrard, B. & Laskar, J. 2003, *Geophysical Journal International*, 154, 970
 Lourens, L., Hilgen, F., Laskar, J., Shackleton, N., & Wilson, D. 2004, in *A Geological Timescale 2004*, ed. F. Gradstein, J. Ogg, & A. Smith, 409–440

- Lourens, L. J., Shuijs, A., Kroon, D., et al. 2005, *Nature*, 435, 1083
- Lourens, L. J., Wehausen, R., & Brumsack, H. J. 2001, *Nature*, 409, 1029
- Lumb, L. I. & Aldridge, K. D. 1991, *Journal of Geomagnetism & Geoelectricity*, 43, 93
- Mignard, F. 1979, *The Moon and the Planets*, 20, 301
- Milankovitch, M. 1941, *Kanon der Erdbestrahlung und seine Anwendung auf das Eiszeitenproblem* (Spec. Acad. R. Serbe, Belgrade)
- Olsen, P. E. & Kent, D. V. 1996, *Palaeogeography, Palaeoclimatology, Palaeoecology*, 122, 1
- Olsen, P. E. & Kent, D. V. 1999, *Royal Society of London Philosophical Transactions Series A*, 357, 1761
- Pälike, H. & Hilgen, F. 2008, *Nature Geoscience*, 1, 282
- Pälike, H., Laskar, J., & Shackleton, N. J. 2004, *Geology*, 32, 929
- Pälike, H., Norris, R. D., Herrle, J. O., et al. 2006, *Science*, 314, 1894
- Poincaré, H. 1910, *Bull.Astron.*, 27, 321
- Quinn, T. R., Tremaine, S., & Duncan, M. 1991, *The Astronomical Journal*, 101, 2287
- Rochester, M. G. 1976, *Geophys.J.R.Astron.Soc.*, 46, 109
- Rubincam, D. P. 1990, *Science*, 248, 720
- Rubincam, D. P. 1995, *Paleoceanography*, 10, 365
- Saha, P. & Tremaine, S. 1994, *Astronomical Journal*, 108, 1962
- Soffel, M., Klioner, S. A., Petit, G., et al. 2003, *Astronomical Journal*, 126, 2687
- Standish, E. M. 1998a, *JPL Interoffice Memorandum*, 98
- Standish, E. M. 1998b, *JPL Planetary and Lunar Ephemerides*
- Sussman, G. J. & Wisdom, J. 1992, *Science*, 257, 56
- van Dam, J. A., Aziz, H. A., Sierra, M. Á. Á., et al. 2006, *Nature*, 443, 687
- Varadi, F., Runnegar, B., & Ghil, M. 2003, *Astrophysical Journal*, 592, 620
- Volland, H. 1978, *Earth's Rotation from Eons to Days*, 62
- Westerhold, T., Röhl, U., Laskar, J., et al. 2007, *Paleoceanography*, 22, 2201
- Westerhold, T., Röhl, U., Raffi, I., et al. 2008, *Palaeogeography, Palaeoclimatology, Palaeoecology*, 257, 377
- Wisdom, J. & Holman, M. 1991, *Astronomical Journal*, 102, 1528
- Zachos, J. C., Shackleton, N. J., Revenaugh, J. S., Pälike, H., & Flower, B. P. 2001, *Science*, 292, 274